Positron cooling by vibrational and rotational excitation of molecular gases

2014 J. Phys. B: At. Mol. Opt. Phys. 47 225209

(http://iopscience.iop.org/0953-4075/47/22/225209)

IOP Publishing Journal of Physics B: Atomic, Molecular and Optical Physics

J. Phys. B: At. Mol. Opt. Phys. **47** (2014) 225209 (10pp) doi:10.1088/0953-4075/47/22/225209

Positron cooling by vibrational and rotational excitation of molecular gases

M R Natisin, J R Danielson and C M Surko

Department of Physics, University of California, San Diego, La Jolla, CA 92093, USA

E-mail: csurko@ucsd.edu

Received 18 June 2014, revised 21 July 2014
Accepted for publication 23 July 2014
Published 4 November 2014

Abstract

Measurements of positron temperature as a function of time are presented when a positron gas, confined in an electromagnetic trap at an elevated temperature ($\geqslant$1200 K), is cooled by interactions with the molecular gases CF_4, N_2 or CO at 300 K. A simple model describing positron thermalization by coupling to vibrational and rotational modes is presented, with cooling-rate predictions calculated in the Born approximation. Comparisons to the measured positron cooling-rate curves permit estimates of the magnitudes of the relevant cross sections. The results are compared with experiment for the case of vibrational excitation, where direct measurements exist; and they provide estimates of the rotational excitation cross sections where direct measurements are not currently possible. Positron cooling rates are compared for these gases at 300 K, and estimates of their effectiveness in cooling positrons to cryogenic temperatures are discussed.

Keywords: positrons, collisions, cooling

(Some figures may appear in colour only in the online journal)

1. Introduction

Positron interactions with matter are important in a variety of contexts, including astrophysics, medicine and material science [1–3]. While a variety of interactions involving relatively high energy positrons have been studied, fewer measurements exist at low temperatures (i.e., $\leqslant$300 K) due to difficulties in obtaining low temperature positrons in large quantities. The advent of trap-based positron beams has enabled the measurement of relatively low energy features, such as state-resolved electronic and vibrational excitations for positron impact on a variety of molecules [4, 5], however direct study of rotational excitation by positron impact is beyond the reach of current technology.

A better understanding of low energy positron–molecule collisions and thermalization processes will aid in the development of novel experimental techniques and technology. In particular, such processes are central to a number of techniques used in creating high-density positron plasmas and tailored positron beams by manipulating plasmas and gases in electromagnetic traps. Prominent examples include the use of molecular gases as an inelastic energy loss mechanism for buffer-gas positron accumulators [6–8], and as the requisite cooling mechanism when rotating electric fields are used to radially compress trapped plasmas the ('rotating wall' (RW) technique) [9–11]. The results of such atomic physics studies could also enable the development of new tools for more precise studies of these low-energy processes (e.g., higher resolution positron beams) [12], and provide key data for detailed simulations of positron cooling (e.g., relevant for modeling the positron dynamics in buffer-gas accumulators and in RW compression) [13, 14].

Positron thermalization in the molecular medium proceeds in several sequential stages. Initially, when the positron temperature is large, the positrons cool rapidly through high energy processes such as electronic excitation and ionization. Once the positron energy falls below the thresholds for these higher energy processes (e.g., a few electron volts), the cooling rate slows dramatically, and the lower energy processes of vibrational and rotational excitation dominate. It is these lower energy processes that are the focus of this paper.

Presented here are measurements and calculations for positron cooling from temperatures $\geqslant$1200 K through inelastic collisions with either CF_4, N_2 or CO gases at 300 K. The positrons are cooled *in situ* in a Penning–Malmberg trap, while being confined by electric and magnetic fields [15].

These molecules were chosen for study to compare the effectiveness in cooling positrons via vibrational and rotational excitation. By symmetry, the permanent dipole and quadrupole moments of CF_4 are zero, leaving vibrational excitation as the dominant cooling channel. For N_2, the cross section for vibrational excitation is small (due to the mode being IR-inactive), and the molecule has no permanent dipole moment, leaving rotational excitation by coupling to the quadrupole moment to dominate. Carbon monoxide has a dipole-active vibrational mode, as well as non-zero dipole and quadrupole moments, allowing it to cool through all three types of vibrational and rotational excitation.

A model is also presented that describes the evolution of the positron temperature during inelastic interactions with a molecular gas. The model predictions, which are calculated using simple cross sections under the Born approximation, are then compared to experimental measurements, allowing estimates of the magnitudes of the relevant cross sections to be made. For the vibrational excitations in CF_4 and CO, these estimates are compared to direct experimental measurements, while for rotational excitations in N_2 and CO, they yield important information, since no direct measurements of the cross sections exist.

This paper is organized as follows. A model of the underlying physical processes and positron cooling is described in section 2. Section 3 gives a brief overview of the experimental apparatus and procedures used to heat the trapped positron gas and to measure positron temperature as a function of time. The results for positron cooling on the three different molecules are presented in section 4, including calculations using the model and estimates regarding the relevant cross sections. Section 5 provides a comparison of the measured data for these molecules, along with a discussion regarding the possible effectiveness of these gases at cooling positrons to cryogenic temperatures. The paper ends with a set of concluding remarks in section 6.

2. Thermalization by inelastic collisions in a molecular gas

Considered here is the process of positron thermalization through inelastic collisions with a molecular gas. The model presented is general, in that it describes the thermalization of positrons (or electrons) with a gas through a variety of inelastic collisions (e.g., vibrational or rotational excitation and de-excitation, etc) provided acceptably accurate forms for the relevant cross sections are available.

The mean positron–molecule collision rate is

$$\langle \Gamma \rangle = n\sqrt{\frac{2}{m}}\,\langle \sigma(\varepsilon)\sqrt{\varepsilon}\,\rangle, \tag{1}$$

where n is the molecule number density, m is the positron mass, $\sigma(\varepsilon)$ is the cross section for the collision, ε is the incident positron energy, and $\langle ... \rangle$ indicates averaging over the positron energy distribution. Since the mass of the molecule is large compared to that of the positron, the molecule is assumed to be stationary, and so only the positron energy is used to describe the relative velocity.

Using (1), the mean collision rate for excitation from, or de-excitation to $(+,-)$ the ith mode can be written

$$\left\langle \Gamma_i^{(+,-)} \right\rangle = n_i\sqrt{\frac{2}{m}}\int_0^\infty \sigma_i^{(+,-)}(\varepsilon)\sqrt{\varepsilon}f(\varepsilon, T)\mathrm{d}\varepsilon, \tag{2}$$

where the cross-sectional average has been written as an integral over the positron energy distribution, $f(\varepsilon, T)$, and n_i is the population density of state i.

If the various states in the molecular are assumed to be Boltzmann distributed, then the population density can be written as

$$n_i \equiv n\frac{g_i \mathrm{e}^{-\frac{E_i}{k_b T_g}}}{\sum_j g_j \mathrm{e}^{-\frac{E_j}{k_b T_g}}}, \tag{3}$$

where g is the mode degeneracy, E is the mode energy, k_b is Boltzmann's constant, and T_g is the temperature of the molecular gas.

The total power transferred to or from the positrons is equal to a sum over all processes which can de-excite or excite the molecule

$$\mathrm{P_{c,h}} = \sum_i \left|\Delta E_i\right| \left\langle \Gamma_i^{(+,-)} \right\rangle. \tag{4}$$

Here the subscripts c and h represent cooling (excitation) and heating (de-excitation) of the positrons, and ΔE_i is the change in energy of the molecule by excitation from, or de-excitation to, state i. The mean rate of energy change of the positrons can then be written

$$\left\langle \frac{\mathrm{d}\varepsilon}{\mathrm{d}t} \right\rangle = -\mathrm{P_{tot}} = \frac{3}{2}k_b\frac{\mathrm{d}T}{\mathrm{d}t}, \tag{5}$$

where

$$\mathrm{P_{tot}} \equiv \mathrm{P_c} - \mathrm{P_h} \tag{6}$$

is the total *cooling* power acting on the positrons.

Using (4)–(6), the first order differential equation describing the evolution of the positron temperature as a function of time is

$$\frac{\mathrm{d}T}{\mathrm{d}t} = -\frac{2}{3k_b}\sum_i \left|\Delta E_i\right|\left(\left\langle \Gamma_i^{(+)} \right\rangle - \left\langle \Gamma_i^{(-)} \right\rangle\right). \tag{7}$$

Assuming the cross sections satisfy detailed balance, the excitation and de-excitation collision rates for each mode will equilibrate at the gas temperature. Above this temperature excitation dominates, cooling the positrons; while below, de-excitation dominates, heating the positrons.

Unfortunately, the dependence of $\mathrm{P_{tot}}$ on the positron temperature cannot be expressed in simple form if it is required that the cross sections used satisfy detailed balance, and so the solution to (7) must be found numerically. For all of the cases considered here, the solutions were found by numerically integrating (7) using a 10 μs time step. Reducing the time step by three orders of magnitude (10 ns) yields a

change in the results of less than 1%, indicating that stable numerical solutions are reached using 10 μs time steps.

For simplicity, it is assumed that the positron energy distribution, $f(\varepsilon, T)$, remains Maxwellian at all times. While no effort is made here to justify this assumption theoretically, the measured positron energy distributions at each temperature (see below) indicate that it is a reasonable approximation.

For the results discussed here, generic formulae for cross sections in the Born approximation are used for the vibrational and rotational excitations and de-excitations. The dominant CF_4 and CO vibrational cross sections are available from experimental measurements, and fit well to simple scalings of the Born-dipole cross sections [16], thus indicating that the use of these cross sections in modeling the vibrational interactions with these species is appropriate. No direct measurements of the rotational cross sections exist for positron impact; however the Born approximation is expected to be approximately valid at the low values of positron energy studied here, where the positron de Broglie wavelengths are large. Additionally, data for rotational excitation of N_2 by *electron* impact suggest that the Gerjuoy–Stein cross sections are reasonably accurate [17].

3. Description of the experiments

The experimental apparatus has been described in detail elsewhere [18]. High energy positrons from a ^{22}Na radioactive source are moderated by inelastic collisions with a thin layer of solid Ne at ~8 K, slowing the positrons to electron-volt energies. These moderated positrons are then magnetically guided into a three stage buffer-gas trap (BGT).

The BGT consists of a modified Penning–Malmberg trap in a ~0.1 T magnetic field. A trapping gas, typically N_2, is injected into the first stage and maintained at lower pressures in the other two stages by differential pumping. The positrons enter the trap on the high pressure side and lose energy through inelastic collisions with the trapping gas, becoming confined in a potential well in the third stage. The cooling gas being studied is injected into the third stage to interact with the trapped positrons, eventually cooling them to the gas temperature (~300 K). For all experiments discussed here, the N_2 trapping gas was maintained at significantly lower pressure in the third stage as compared with that of the cooling gas, so that the positrons cooled predominantly through interactions with the cooling gas. Data were taken at two different N_2 pressures to verify this.

Once the trapped positrons have cooled to the ambient gas temperature of 300 K, Gaussian noise with an amplitude of 150–500 mV peak-to-peak and a bandwidth of 9 MHz is applied to one of the confining electrodes for 100–200 ms, then shut off, at which point the positron temperature is between ~1200–1800 K, depending on the molecule being studied. The peak temperature reached during this process is determined by a competition between the rf heating and gas cooling rates, and so these initial conditions were varied for each gas in an attempt to reach reasonably similar peak temperatures. The temperature of the positrons is then measured as a function of time as they relax to the ambient gas temperature. These measurements are done by raising the bottom of the potential well, lifting the positrons over a potential barrier, and forming a pulsed positron beam [4, 12, 19].

This beam is then passed through a retarding potential analyzer (RPA), where the beam parallel energy distribution is measured. This measurement is then repeated with the RPA in a different magnetic field, and the two measured energy distributions are fit to an experimental beam energy distribution function, which consists of a Gaussian convolved with a Maxwellian [18], to obtain the mean parallel energy of the beam at each magnetic field.

The two measured mean parallel energies, along with the magnetic fields in which they were measured, are related to their respective mean perpendicular energies through energy conservation and the invariance of the positron orbital magnetic moment [20, 21], yielding

$$\overline{E}_{\perp} = \frac{\overline{E}'_{\parallel} - \overline{E}_{\parallel}}{1 - B'/B}, \tag{8}$$

where $\overline{E}_{\perp}$ and $\overline{E}_{\parallel}$ represent the mean perpendicular and parallel energies of the positrons in the RPA, B is the magnetic field in the RPA region, and the primes distinguish parameters evaluated at the second value of the magnetic field.

The mean perpendicular energy of the positrons in the BGT, $\overline{E}^{\mathrm{t}}_{\perp}$, can then be obtained from the measured $\overline{E}_{\perp}$ in the RPA region by

$$\overline{E}^{\mathrm{t}}_{\perp} = \overline{E}_{\perp}\frac{B^{\mathrm{t}}}{B}, \tag{9}$$

where B^{t} and B are the magnetic fields in the BGT and RPA regions, respectively. Combining (8) and (9) and using the fact that $T_{\parallel} = T_{\perp} \equiv T = \overline{E}^{t}_{\perp}/k_b$ in the BGT before the beam is formed gives the temperature of the positrons in the trap

$$T = \frac{\overline{E}'_{\parallel} - \overline{E}_{\parallel}}{k_b\left(1 - B'/B\right)}\left(\frac{B^{\mathrm{t}}}{B}\right). \tag{10}$$

Equation (10) is the basis for the temperature measurements presented here. Note that this relation assumes that the perpendicular energy of the positrons is not affected by the beam formation process (i.e., $\overline{E}_{\perp}$ changes only due to the positrons moving through a changing magnetic field). Computer simulations of the beam formation process have been done to verify that this is indeed the case.

Examples of measured parallel energy distributions used to determine the positron temperature using (10) are shown in figure 1. The points show the measured integrated parallel energy distributions with the RPA in a magnetic field of $B \sim 800$ Gauss and $B' = B/4$. The dashed lines show fits to the data, providing the mean parallel energies, $\overline{E}_{\parallel}$ and $\overline{E}'_{\parallel}$, represented by the vertical dotted lines in figures 1 (a) and (b), respectively. For the example shown, (10) gives a temperature of ~717 ± 20 K. Also shown by the solid lines are the derivatives of the fits, which represent the respective parallel energy distributions.

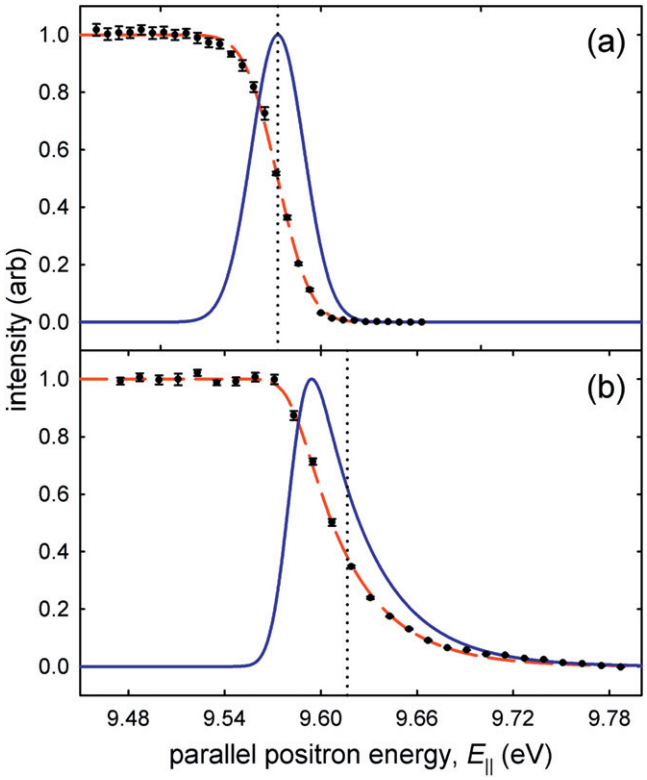

Figure 1. Examples of the parallel energy distributions, measured at two values of RPA magnetic field, that are used to calculate the positron temperature (a) $B \sim 800$ G, and (b) $B' \sim 200$ G; (•) measured integrated parallel energy distributions, (- - -) fits to data, and (—) derivatives of fits that represent the positron energy distributions. (·····) vertical lines represent fitted mean parallel energies $\overline{E}_{\|}$ and $\overline{E}'_{\|}$.

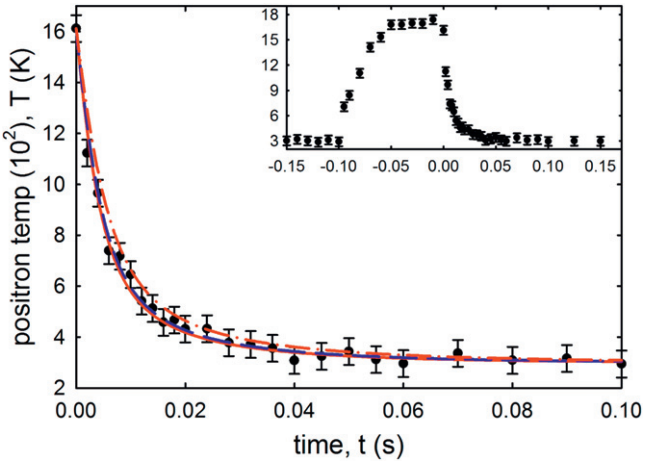

Figure 2. Positron cooling with $0.51 \pm 0.05\,\mu$Torr of CF_4 at 300 K: (•) measured data, (—) solution to (7) for vibrational (de-)excitation of the ν_3 mode; and (- - - -) solution to (7) with cross sections scaled up by a fitting factor $\eta = 0.95$ and (- - - -) solution to (7) with cross sections scaled by $\eta = 0.75$ to match the direct measurement given in [16]. Inset shows full heating and cooling cycle.

These and similar measurements are found to be consistent with the assumption of the model that the positron energy distribution remains Maxwellian, even while the positrons are being heated or cooled. The beam formation process removes most of the information regarding the original parallel positron energies, but leaves the perpendicular energies intact. As seen in figure 1(a), when the RPA magnetic field is comparable to that of the buffer gas trap, the parallel energy distribution resembles a Gaussian. As the RPA field is lowered, some positron perpendicular energy is transferred into the parallel component due to the invariance of the orbital magnetic moment. This results in an increase in the mean parallel energy, as well as the development of a high energy tail in the parallel energy distribution (cf figure 1 (b)). At all temperatures discussed here, the measured distributions fit well with the Gaussian–Maxwellian distribution function, indicating that the positrons equilibrate rapidly to a Maxwellian distribution even while being heated or cooled.

For the results presented here, ∼20 000 positrons were used with a magnetic field ratio $B'/B = 1/4$. Pressure measurements were done using an ion gauge calibrated to a capacitance manometer placed *in situ* in the trapping region, with an overall uncertainty of 10%. Measurements with each gas at half pressure were done at several temperatures to ensure that the cooling rates varied linearly with the gas pressure, indicating that there were no gas-independent cooling mechanisms present. Since the time required for each temperature measurement is significant (∼1 h), multiple measurements of each data point was not practical. For this reason, the error bars shown for each molecule represent the standard deviation of five measurements of the $t = 0$ s point, where the error is expected to be largest.

4. Results

4.1. Carbon tetrafluroide

The first case considered is positron cooling through interactions with CF_4 at a pressure of $0.51 \pm 0.05\,\mu$Torr. The measured positron temperature during the heating and cooling cycle is shown in the inset of figure 2. The positrons were trapped and initially allowed to cool to the gas temperature of ∼300 K, after which rf heating noise was applied for 100 ms. The positrons reached a peak temperature of ∼1700 K, at which point the noise was switched off, and the positrons allowed to relax back to the gas temperature.

Both the permanent electric dipole and quadrupole moments of CF_4 are zero by symmetry, leaving vibrational excitation by coupling to the transition dipole moments as the dominant cooling channel. The cross section used is the Born-dipole cross section [22], with the de-excitation cross section obtained by requiring detailed balance

$$\sigma_{0,\nu} = \frac{8\pi a_0^2}{3} g_\nu \left(\frac{\mu_\nu}{e a_0}\right)^2 \left(\frac{R_y}{\varepsilon}\right) \ln\left[\frac{\sqrt{\varepsilon} + \sqrt{\varepsilon - \varepsilon_\nu}}{\sqrt{\varepsilon} - \sqrt{\varepsilon - \varepsilon_\nu}}\right],$$
$$\sigma_{\nu,0} = \frac{8\pi a_0^2}{3} g_0 \left(\frac{\mu_\nu}{e a_0}\right)^2 \left(\frac{R_y}{\varepsilon}\right) \ln\left[\frac{\sqrt{\varepsilon + \epsilon_\nu} + \sqrt{\epsilon}}{\sqrt{\varepsilon + \epsilon_\nu} - \sqrt{\epsilon}}\right], \qquad (11)$$

where a_0 is the Bohr radius, R_y is the Rydberg (13.6 eV), ε is

the positron energy, μ_ν is the transition dipole moment with dimensions of ea_0, and g_ν and ε_ν are the degeneracy and energy of mode ν. Here, $\sigma_{0,\nu}$ describes excitation from the ground state to the first excited state ν, and $\sigma_{\nu,0}$ represents de-excitation from state ν. Excitations from excited states are neglected.

There are two triply degenerate, dipole-active CF_4 vibrations; the ν_3 degenerate stretch mode at $\varepsilon_\nu = 159$ meV, and the ν_4 degenerate deformation mode at $\varepsilon_\nu = 78.4$ meV. The transition dipole moments for these modes, which are calculated using the absolute integrated intensities and procedures given by Bishop and Cheung in [23], are found to be 0.12 ea_0 and 0.02 ea_0 for the ν_3 and ν_4 modes, respectively. Since the cross sections scale as μ_ν^2, the contribution from the weak ν_4 mode is small, and so only (de-)excitation of the ν_3 mode is considered here.

As shown in figure 2, even at the low gas pressure of 0.51 μTorr, the positrons thermalize with the CF_4 remarkably quickly, reaching 300 K in under 50 ms. Also shown as a solid line is the solution to (7) for the case of (de-)excitation of the ν_3 vibrational mode using the cross sections given by (11). In this case the simple model is in excellent agreement with the measured data.

The measured positron cooling curve also provides some information regarding the cross sections for the relevant interactions. The fact that the model prediction matches well for CF_4 suggests that the Born-dipole cross section is a good approximation to the actual cross section. Applying a constant empirical scale factor, η, to both the excitation and de-excitation cross sections given by (11) enables an estimate of the vibrational cross section. For the case of CF_4, the best fit is found by scaling the Born-dipole cross sections by a factor $\eta = 0.95 \pm 0.10$ resulting in the curve shown by the dashed line in figure 2.

For comparison, the ν_3 vibrational excitation cross section for positron impact on CF_4 has been directly measured experimentally and found to be a factor of $\sim 0.75 \pm 0.2$ times the Born-dipole model prediction [16]. The positron cooling curve obtained from the model using this scale factor is shown by the dot-dashed curve in figure [4]. The fact that the two measurements lie within their respective error bars confirms that the positron cooling curves may be used to estimate the underlying cross sections. While this technique does not provide as detailed cross section information as direct measurement, it is a useful alternative, particularly in cases where direct measurement is not currently possible.

4.2. Molecular nitrogen

Data for N_2 at a pressure of 15 ± 1.5 μTorr are shown in figure 3. Since N_2 is a homonuclear diatomic molecule, it has no permanent dipole moment and the vibrational mode is dipole-inactive. Thus, the lowest order coupling is rotational excitation via the non-zero quadrupole moment. In this case, the selection rules allow only rotational transitions with $\Delta j = \pm 2$. The cross sections for excitation from and de-excitation to rotational state j in the Born approximation are described by the Gerjuoy–Stein equations [25]

$$\sigma_{j,j+2} = \frac{8\pi a_0^2}{15}\left(\frac{Q}{ea_0^2}\right)^2 \frac{(j+2)(j+1)}{(2j+3)(2j+1)}\sqrt{1-\frac{\Delta\varepsilon_j}{\varepsilon}},$$

$$\sigma_{j+2,j} = \frac{8\pi a_0^2}{15}\left(\frac{Q}{ea_0^2}\right)^2 \frac{(j+2)(j+1)}{(2j+3)(2j+5)}\sqrt{1+\frac{\Delta\varepsilon_j}{\varepsilon}}, \qquad (12)$$

where Q is the quadrupole moment with dimensions of ea_0^2. The energies of the rotational states are $\varepsilon_j = B_r j(j+1)$, with B_r the rotational constant of the molecule, and so the energy transferred to and from the positron following a collision is $\Delta\varepsilon_j = B_r(4j+6)$.

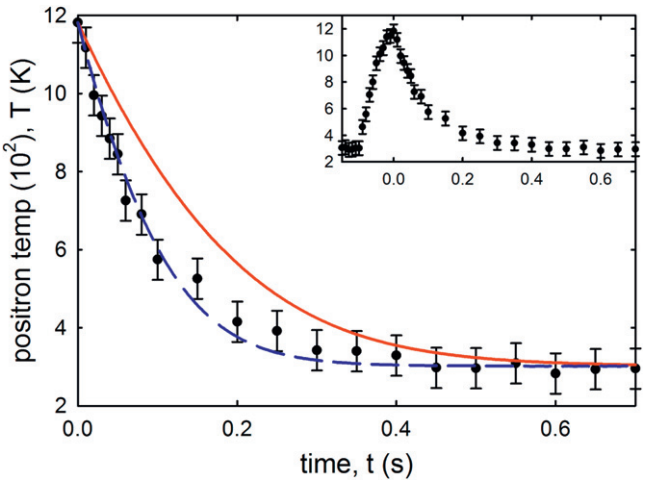

Figure 3. Positron cooling with 15 ± 1.5 μTorr of N_2 at 300 K: (•) measured data; (—) solution to (7) for quadrupole rotational (de-) excitation of all contributing j rotational states; and (- - - -) solution to (7) with cross sections scaled up by $\eta = 1.8$. The inset shows the full heating and cooling cycle.

As shown in figure 3, the positrons thermalize with N_2 much more slowly than for CF_4, even with the significantly higher gas pressure and lower initial positron temperature, taking ~ 0.5 s to reach 300 K. The prediction from (7), using the cross sections given by (12) with $Q = 1.27$ ea_0^2 and $B_r = 0.25$ meV [25, 26], is shown by the solid curve. All rotational states up to $j = 60$ are included in the calculation, though the contributions from $j \gtrsim 30$ are negligible, and the degeneracy is taken to be $6(2j+1)$ and $3(2j+1)$ for even and odd j, respectively.

In this case, the calculated cooling rate is lower than seen in the measured data, suggesting that the Gerjuoy–Stein formula underestimates the rotational excitation cross sections for N_2 by positrons. Since the Born approximation involves only long range effects, this may indicate that short range effects, such as polarization, are important in describing positron collisions with N_2 [27]. It should be noted that, while the N_2 vibrational mode is dipole-inactive and therefore has a cross section of zero in the Born approximation, more sophisticated calculations predict a non-zero vibrational excitation cross section. However, the magnitude of the predicted cross section is small, approximately three orders of magnitude smaller than that for CF_4 [28, 29]; including this process in the model does not significantly affect the positron cooling rate.

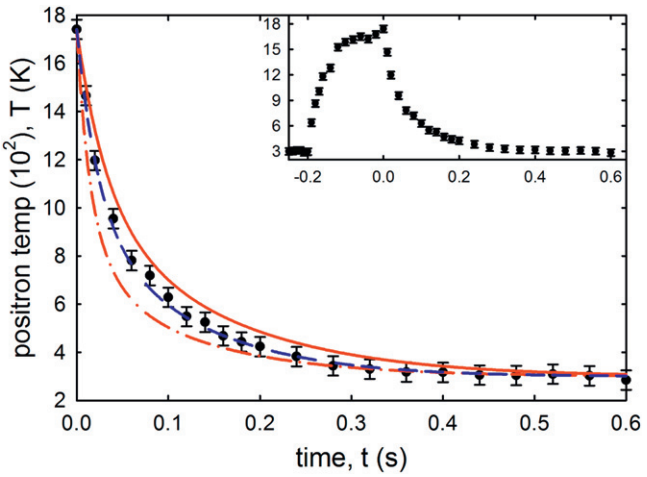

Figure 4. Positron cooling with $1.7 \pm 0.2\,\mu$Torr of CO at 300 K: (•) measured data; (—) solution to (7) for vibrational, dipole rotational and quadrupole rotational (de-)excitation of the ν_1 mode and all contributing j rotational states; (— ·—) solution to (7) with vibrational cross sections scaled by $\eta = 2.8$ to match direct measurement given in [16]; and (- - - -) solution to (7) with vibrational, dipole and quadrupole rotational cross sections scaled by $\eta = 1.5$, 1.5 and 1, respectively.

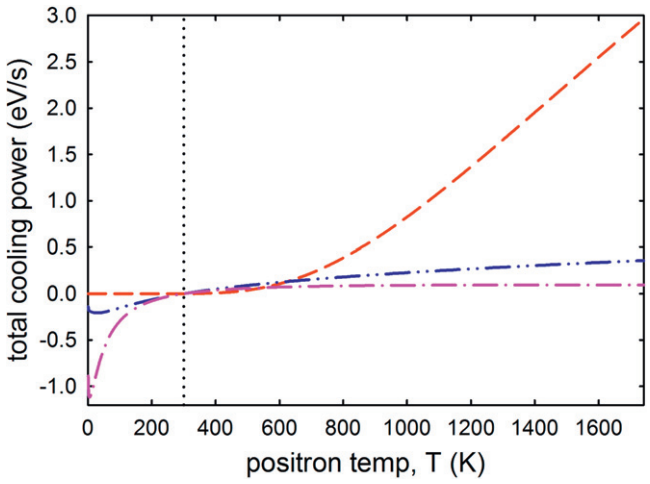

Figure 5. Total cooling power (defined in (6)) as a function of the positron temperature for 1.74 μTorr of CO at a gas temperature of 300 K (vertical dotted line) for (- - - -) vibrational excitation, (—·—) dipole coupled rotations and (— ··—) quadrupole coupled rotations.

Adjusting the magnitude of the rotational (de-) excitation cross sections given by (12) yields a best fit scale factor $\eta = 1.8 \pm 0.2$ (dashed curve in figure 3). This measurement yields a magnitude for the $j = 0 \rightarrow 2$ rotational excitation cross section which is in reasonable agreement with more recent theoretical calculations [30], however it should be noted that the energy dependence of the Gerjuoy–Stein formulae are markedly different than predicted by these calculations. Since no direct measurements of the rotational excitation cross section for positrons on N_2 exist, the indirect measurements shown in figure 3 represent a potentially important benchmark for comparison to future theoretical calculations.

4.3. Carbon monoxide

Cooling data for CO at a pressure of $1.7 \pm 0.2\,\mu$Torr are shown in figure 4. Unlike the previous two cases, CO has both non-zero permanent dipole and quadrupole moments, as well as a dipole active vibrational mode. The solution to (7) then involves both the vibrational and quadrupole rotational interactions given by (11) and (12), as well as additional cross sections describing rotational interactions by coupling to the permanent electric dipole moment. For dipole-coupled rotations, the allowed transitions are $\Delta j = \pm 1$. Again using the Born approximation, they are [32]

$$\sigma_{j,j+1} = \alpha\left(\frac{R_y}{\varepsilon}\right)\left(\frac{j+1}{2j+1}\right)\ln\left[\frac{\sqrt{\varepsilon} + \sqrt{\varepsilon - \Delta\varepsilon_j}}{\sqrt{\varepsilon} - \sqrt{\varepsilon - \Delta\varepsilon_j}}\right],$$
$$\sigma_{j+1,j} = \alpha\left(\frac{R_y}{\varepsilon}\right)\left(\frac{j+1}{2j+3}\right)\ln\left[\frac{\sqrt{\varepsilon + \Delta\varepsilon_j} + \sqrt{\varepsilon}}{\sqrt{\varepsilon + \Delta\varepsilon_j} - \sqrt{\varepsilon}}\right], \qquad (13)$$

with

$$\alpha \equiv \frac{8\pi a_0^2}{3}\left(\frac{\mu}{e a_0}\right)^2, \qquad (14)$$

where μ is the permanent dipole moment with dimensions of $e a_0$. Here, the energy exchanged with the positron in each collision is $\Delta\varepsilon_j = 2B_r(j+1)$.

For CO, the rotational constant B_r is 0.24 meV [26], and the permanent dipole and quadrupole moments are 0.044 $e a_0$ and 2.59 $e a_0^2$, respectively [25, 32]. The only vibrational mode is the dipole-active C-O stretch mode, occurring at $\varepsilon_\nu = 266$ meV with a transition dipole moment of 0.042 $e a_0$ [23].

Shown in figure 4 by a solid line is the prediction of (7) using the cross sections given by (11), (12), and (13). For this calculation all states up to $j = 60$ were included for both the dipole and quadrupole coupled rotations. The predicted cooling rate is surprisingly close to that measured, given the simplicity of the model and the variety of open cooling channels.

The total cooling power for each of the three processes is plotted in figure 5. Note that it switches sign from >0 to <0 when the positron temperature decreases below the gas temperature (300 K). Not surprisingly, the cooling power is dominated by vibrational excitation at high temperatures. However, at $T \sim 600$ K, the contribution from quadrupole-coupled rotations becomes comparable. Interestingly, due to the large quadrupole moment of CO, and the fact that the allowed transitions for quadrupole coupling are $\Delta j = \pm 2$, quadrupole rotational excitations contribute more to the positron cooling than do the dipole-coupled rotations over the entire temperature range studied.

While no measurements exist for rotational excitation of CO by positron impact, the vibrational excitation cross section has been measured and found to be 2.8 ± 0.6 times larger than that predicted by Born-dipole coupling [16]. The

dot-dashed curve shown in figure 4 shows the calculated cooling rate with this scaling applied to the Born-dipole cross section, leaving the rotational cross sections unscaled.

Unlike the previous cases of CF_4 and N_2, CO involves multiple types of interaction, and so determining the magnitudes of the underlying cross sections by fitting the measured data using a single scale factor is more complicated. However, the large difference in the strengths and energies of the vibrational interactions relative to that of the rotational interactions allows rough estimates of their respective magnitudes to be made based on the shape of the cooling curve.

Fitting the measured data in the range of temperatures above 800 K, where the positron cooling is dominated by vibrational excitation, suggests that the Born-dipole vibrational cross section should be scaled by $\eta \sim 1.5$. Given the additional uncertainties in this factor due to potential contributions from the rotational modes, this result is in reasonable agreement with the direct measurement of 2.8. Since the dipole and quadrupole rotational interactions occur at similar energies, the scale factors for their cross sections cannot be determined individually. Nevertheless, relatively crude estimates of the ranges of cross-section values can be made. If the dipole rotations are assumed to be completely absent, then the quadrupole rotational cross sections must be enhanced by a factor of ~1.5 to agree with the data. Alternatively, if the quadrupole interactions were assumed absent, then the dipole rotational cross sections would need to be scaled up by ~3.

Therefore, the data suggests that the Born-dipole rotational cross sections given by (13) should be scaled by $\eta \sim 0$–3.5, while the quadrupole rotational cross sections given by (12) require $\eta \sim 0$–1.5. Indeed, calculations from [33, 34] indicate that the dipole rotational excitation cross section should be scaled by a factor of ~1–2, while the quadrupole rotational excitation cross section should be scaled by a factor of ~0.3. As an example, the dashed curve in figure 4 represents the solution with the cross section for vibrations, dipole rotations and quadrupole rotations scaled by $\eta = 1.5$, 1.5 and 1, respectively.

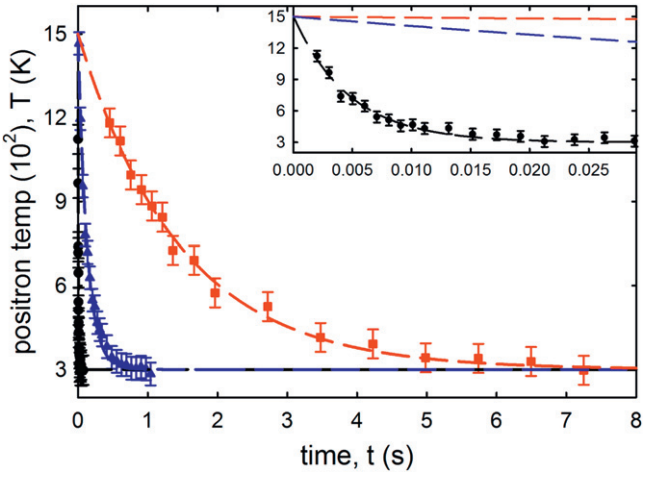

Figure 6. Positron cooling with (•) CF_4, (▲) CO, and (■) N_2 gases at 300 K normalized to 1 μTorr and shifted to line up at $t = 0$ s; and (- - - -) an exponential fit for each case. Inset shows CF_4 in more detail.

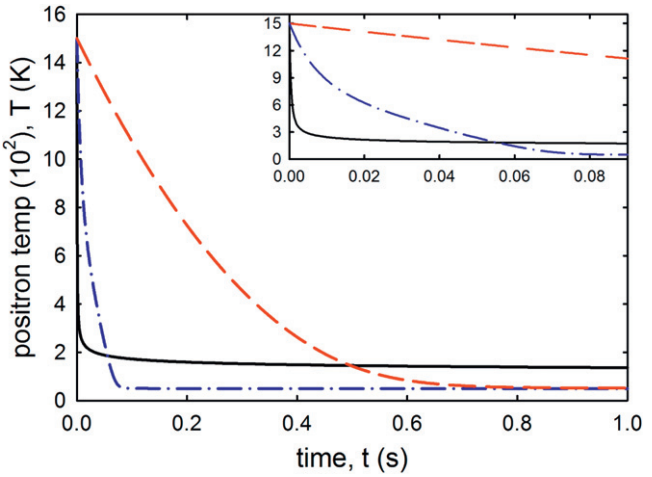

Figure 7. Solutions to (7) for a gas pressure of 1 μTorr and a temperature of 50 K using cross sections scaled by the empirically determined scale factors, η, listed in table 1 for the (—) CF_4, (- - - -) N_2 and (—·—) CO. Inset shows CF_4 and CO curves in more detail. See text for details.

5. Discussion

Measurements of positron thermalization with several different molecular gases at 300 K have been presented and compared to the predictions of a simple model. The positron cooling curves agree well with model predictions using generic cross sections in the Born approximation, scaled by constant numerical factors. In this section, the results from section 4 are compared and discussed, followed by a discussion of the effectiveness of these gases for cooling to cryogenic temperatures.

5.1. Comparisons

The time scales in which the positrons thermalize with a molecular gas clearly depends strongly on the type of gas and the cooling channels available. For comparison, figure 6 shows the measured cooling curves for the three molecules studied, normalized to a gas pressure of 1 μTorr. Also shown are exponential fits over this temperature range for each of the molecules. While the cooling curves are not quite exponential in shape, these fits allow estimates of the pressure-normalized 1/e times for these gases.

The model parameters used and the characteristic cooling times for the three molecules studied are listed in table 1. By far the most effective cooling gas over the temperature range studied is CF_4, with a pressure-normalized 1/e time, τ_p, of just 4.8 ms–μTorr ; a factor of ~300 times faster than that of N_2. The total cooling power for CF_4 is significantly larger than that of either N_2 or CO over all temperatures studied (i.e., above 300 K). This is due to the very large transition dipole moment of the ν_3 vibrational mode, as well as the relatively high energy of this mode, which acts to remove significant energy from the positrons with each collision.

With a 1/e time of 1.5 s at 1 μTorr, N_2 is the least effective cooling gas studied. Both the cross sections and the amount of energy transferred are significantly smaller in the case of quadrupole rotational excitation than for that of vibrational excitation, resulting in far slower positron cooling. In addition, the quadrupole moment of N_2 is more than a factor of two smaller than that of CO, resulting in a smaller cooling power even at low temperatures where the CO vibration becomes insignificant.

The molecule CO cools through both vibrational and rotational excitation, and so it is expected to maintain reasonable cooling power over a broader range of temperatures than either CF_4 or N_2. However, the non-degenerate C-O stretch vibration has a transition dipole moment which is ~3 times smaller than that of the triply degenerate CF_4 stretch mode, making its vibrational excitation cross section ~27 times smaller.

5.2. Cooling positrons to cryogenic temperatures

The formation of trap-based beams using positrons cooled to cryogenic temperatures would enable studies of many new physical processes, such as direct measurement of rotational excitations and new studies of positron–molecule annihilation mechanisms [12]. While the measurements discussed here were done with a gas temperature ~300 K, they provide insight into the effectiveness of these gases in cooling positrons to cryogenic temperatures.

All three molecules studied are expected to have a reasonable vapor pressure (>1 μTorr) at 50 K, and so they are all possible candidates for use as a cryogenic cooling gas. The data suggest that vibrational excitation is by far the most effective method of cooling positrons to 300 K. However, as the positron temperature decreases, so does the effectiveness of this cooling channel, due to the relatively high energies of vibrational modes. This raises the question as to whether rotational excitations are able to cool positrons to low temperatures on reasonable time scales.

Figure 7 shows the solution to (7) for positron cooling on CF_4, N_2 and CO at a pressure of 1 μTorr and a temperature of 50 K. Note that fixing the gas pressure at 1 μTorr and reducing the temperature from 300 K to 50 K results in a factor of 6 increase in the gas number density, yielding far faster cooling rates. For these calculations, the Born approximation scale factors listed in table 1 for CF_4 and N_2 were applied to the respective cross sections, while for CO, a factor of 1.5 was applied to the vibrational and dipole rotational cross sections, leaving the quadrupole rotational cross sections unscaled. Figure 8 shows the total cooling power, defined by (6), under these conditions.

As in the 300 K case (figure 6), the positrons cool remarkably rapidly through interactions with CF_4. However, due to the relatively high energy of the ν_3 vibrational mode in CF_4, the cooling power drops off rapidly as the positron temperature falls. By 130 K the cooling power has dropped below 1 meV s^{-1}, making cooling below this temperature impractical on reasonable time scales. It should be noted that the lower energy ν_4 degenerate deformation mode, occurring at 78.4 meV, will make a non-negligible contribution to the cooling curve at very low temperatures. This mode was neglected due to having an excitation cross section which is a factor of ~20 smaller than that of the ν_3 mode, however at temperatures below ~230 K it becomes the dominant cooling mechanism, allowing the positrons to cool to $\lesssim$100~K on reasonable time scales (not shown).

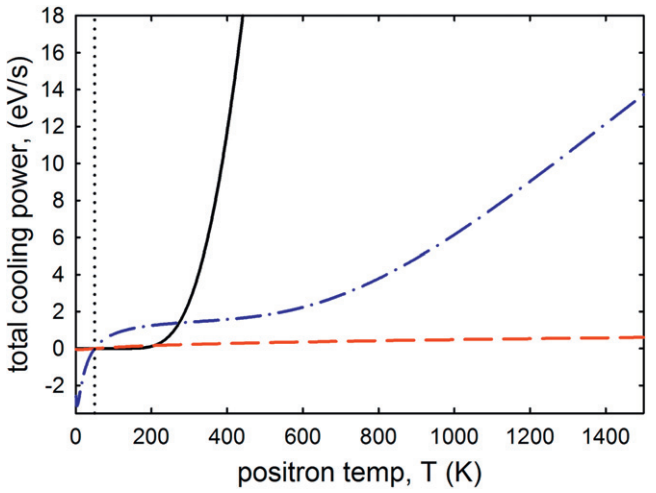

Figure 8. Calculated total cooling power, defined as in (6), for the conditions described in figure 7 for (—-) CF_4, (- - - -) N_2 and (—·—) CO. Vertical dotted line shows gas temperature. See text for details.

Referring to figure 8, N_2 again shows a comparatively weak cooling power over a majority of the temperature range. However, because of the low energies of the rotational modes, occurring at $\varepsilon_j = 1.5$ meV for the lowest excited rotational state of N_2, reasonable cooling power continues to very low temperatures. Below ~210 K, N_2 becomes a better cooling gas than CF_4, and it appears to cool the positrons to 50 K in ~1 ms at 1 μTorr.

As was seen in figure 5 and can also be seen by the change in slope of the CO curve in figures 7 and 8, CO transitions from cooling predominantly through vibrational excitations to rotations at ~600 K, and becomes the most effective cooling gas of the three discussed here at temperatures $\lesssim$270 K. Due to its larger quadrupole and dipole moments, and its dipole-active vibrational mode, CO maintains a larger cooling power than N_2 over all temperatures. This, along with the presence of its vibrational mode at high energies, enables it to cool positrons from 1500 K to 50 K in $\lesssim$100 ms.

6. Concluding remarks

Measurements of positron cooling with three different molecular gases have been presented. These measurements show the effectiveness of cooling positrons through vibrational and rotational excitation. While all three gases can be used to cool positrons to 300 K on reasonable time scales, CF_4 proved to be the fastest, followed by CO, with N_2 the slowest of the molecules studied.

Table 1. Parameters for the three molecules studied here: B_r is the rotational constant; μ and Q are the permanent electric dipole and quadrupole moments; ϵ_ν and μ_ν are the vibrational mode energies and transition dipole moments; τ_p is the pressure normalized 1/e time constant from figure 6; η are empirical scale factor(s) for the relevant theoretical cross sections required to obtain agreement with experiment. For the case of CO, η is given for the dipole/quadrupole/vibrational cases, respectively. See text for details.

Molecule	B_r (meV)	μ (ea_0)	Q (ea_0^2)	ϵ_ν (meV)	μ_ν (ea_0)	τ_p (ms μTorr)	η
CF_4	—	0	0	159	0.12	4.8	0.95 ± 0.1
N_2	0.25	0	1.27	—	—	1500	1.8 ± 0.2
CO	0.24	0.044	2.59	266	0.042	130	~0–3.5/0–1.5/1.5

A simple model was introduced to describe positron thermalization through inelastic collisions and used to calculate the positron temperature as a function of time. For comparison with the measurements, generic cross sections in the Born approximation were used for vibrational, dipole-rotational and quadrupole-rotational excitation and de-excitation. Using these cross sections, the model showed excellent agreement with measurements of CF_4, while both CO and N_2 appear to cool faster than suggested by the Born approximation. Vibrational excitation provided the most effective cooling mechanism at higher positron temperatures, due to typically larger cross sections and mode energies, and this mechanism provides adequate cooling power even down to 300 K.

Comparisons between model predictions and measurements were also used to provide an estimate of the magnitudes of the relevant cross sections by scaling the Born cross sections by constant numerical factors. It was found that the CF_4 results fit well with the measurements using the Born-dipole cross sections for vibrational excitation, while the CO vibrations required a scaling factor of ~1.5. These results are in reasonable agreement with direct experimental measurements, which show that the CF_4 ν_3 excitation is within 25% of Born-dipole, while the CO vibration is enhanced above the Born-dipole result by ~2.8 [16]. Due to the inherent complexities involved in extracting cross section data from the measured cooling curves, this technique is not a replacement for direct measurements of the cross sections themselves. However this method is useful in providing estimates of the cross sections where direct measurement cannot be done.

In the case of N_2, the data indicate that the Gerjuoy–Stein cross sections are good to within a factor of two. This is in contrast to the case of electron collisions where these cross sections are found to be reasonably accurate [17]. This difference may be due to the fact that, in the positron case, short-range effects may be important in describing these interactions, in accord with the conclusions of [35].

Lastly, the model was used to predict the effectiveness of these gases in cooling positrons to cryogenic temperatures. While CF_4 should allow rapid cooling to ~100 K, its vibrational excitation is ineffective in cooling below this temperature. In contrast, both N_2 and CO should allow cooling to $\lesssim$50 K on reasonable time scales through rotational excitation, making them excellent candidates for use as cryogenic cooling gases.

As mentioned above, one important use of the cooling processes studied here is for the development of advanced trap-based techniques to tailor the accumulation, storage and delivery of low-energy positrons for a variety of end uses. It is clear from the results presented here that more accurate modeling of the interaction of positrons with molecular gases (e.g., [13, 14, 36]) will hinge on more precise measurements of the relevant cross sections. This is particularly the case for rotational excitation, where presently, no direct measurements exist.

Acknowledgments

We wish to acknowledge helpful conversations with Gleb Gribakin and Jonathan Tennyson and the expert technical assistance of E A Jerzewski. This work is supported by the US National Science Foundation, grant PHY 10-68023.

References

[1] Guessoum N, Jean P and Gillard W 2010 Positron annihilation on polycyclic aromatic hydrocarbon molecules in the interstellar medium *Mon. Not. R. Astron. Soc.* **402** 1171–8
[2] Wahl R L (ed) 2002 *Principles and Practice of Positron Emission Tomography* (Philadelphia, PA: Williams & Wilkins)
[3] Gidley D W, Peng H-G and Vallery R S 2006 Positron annihilation as a method to characterize porous materials *Annu. Rev. Mater. Sci.* **36** 49–79
[4] Sullivan J P, Gilbert S J, Marler J P, Greaves R G, Buckman S J and Surko C M 2002 Positron scattering from atoms and molecules using a magnetized beam *Phys. Rev.* A **66** 042708
[5] Surko C M, Gribakin G F and Buckman S J 2005 Low-energy positron interactions with atoms and molecules *J. Phys. B: At. Mol. Opt. Phys.* **38** 57–126
[6] Greaves R G and Surko C M 1997 Antimatter plasmas and antihydrogen *Phys. Plasmas* **4** 1528–43
[7] Surko C M and Greaves R G 2004 Emerging science and technology of antimatter plasmas and trap-based beams *Phys. Plasmas* **11** 2333–48
[8] Cassidy D B, Deng S H M, Greaves R G and Mills A P Jr. 2006 Accumulator for the production of intense positron pulses *Rev. Sci. Instrum.* **77** 073106
[9] Greaves R G and Surko C M 2001 Radial compression and inward transport of positron plasmas using a rotating electric field *Phys. Plasmas* **8** 1879–85

[10] Danielson J R and Surko C M 2006 Radial compression and torque-balanced steady states of single-component plasmas in penning–malmberg traps *Phys. Plasmas* **13** 055706
[11] Cassidy D B, Greaves R G, Meligne V E and Mills A P 2010 Strong drive compression of a gas-cooled positron plasma *Appl. Phys. Lett.* **96** 101502
[12] Natisin M R, Hurst N C, Danielson J R and Surko C M 2013 Recent progress in tailoring trap-based positron beams *Am. Inst. Phys. Conf. Ser.* **1521** pp 154–64
[13] Marjanovic S, Suvakov M, Bankovic A, Savic M, Malovic G, Buckman S and Petrovic Z 2011 Numerical modeling of thermalization of positrons in gas-filled surko traps *IEEE Trans. Plasmas Sci.* **39** 2614–5
[14] Bankovic A, Marler J P, Suvakov M, Malovic G and Lj Petrovic Z 2008 Transport coefficients for positron swarms in nitrogen *Nucl. Instrum. Methods* B **266** 462–5
[15] Murphy T J and Surko C M 1992 Positron trapping in an electrostatic well by inelastic collisions with nitrogen molecules *Phys. Rev.* A **46** 5696–705
[16] Marler J P, Gribakin G F and Surko C M 2006 Comparison of positron-impact vibrational excitation cross sections with the born-dipole model *Nucl. Instrum. Methods* B **247** 87–91
[17] Robertson A G, Elford M T, Crompton R W and Morrison M A 1997 Rotational and vibrational excitation of nitrogen by electron impact *Aust. J. Phys.* **50** 441–72
[18] Gribakin G F, Young J A and Surko C M 2010 Positron-molecule interactions: Resonant attachment, annihilation, and bound states *Rev. Mod. Phys.* **82** 2557–607
[19] Gilbert S J, Kurz C, Greaves R G and Surko C M 1997 Creation of a monoenergetic pulsed positron beam *Appl. Phys. Lett.* **70** 1944–6
[20] Chen F F 1984 *Introduction to Plasma Physics and Controlled Fusion Volume I Plasma Physics* 2nd edn (New York: Springer)
[21] Young J A and Surko C M 2006 Charged particle motion in spatially varying electric and magnetic fields *Nucl. Instrum. Methods* B **247** 147
[22] Itikawa Y 1974 The born cross section for vibrational excitation of a polyatomic molecule by electron collisions *J. Phys. Soc. Japan* **36** 1121–6
[23] Bishop D M and Cheung L M 1982 Vibrational contributions to molecular dipole polarizabilities *J. Phys. Chem. Ref. Data* **11** 119–33
[24] Gerjuoy E and Stein S 1955 Rotational excitation by slow electrons *Phys. Rev.* **97** 1671–9
[25] Graham C, Imrie D A and Raab R E 1998 Measurement of the electric quadrupole moments of CO_2, CO, N_2, CL_2 and BF_3 *Mol. Phys.* **93** 49–56
[26] Huber K P and Herzberg G (ed) 1979 *Molecular Spectra and Molecular Structure IV. Constants of Diatomic Molecules* (New York: Van Nostrand Reinhold)
[27] Takayanagi K and Inokuti M 1967 On the scattering of slow positrons by molecules *J. Phys. Soc. Japan* **23** 1412–4
[28] Mazon K T, Tenfen W, Michelin S E, Arretche F, Lee M-T and Fujimoto M M 2010 Vibrational cross sections for positron scattering by nitrogen molecules *Phys. Rev.* A **82** 032704
[29] Gianturco F A and Mukherjee T 1997 Dynamical coupling effects in the vibrational excitation of H_2 and N_2 colliding with positrons *Phys. Rev.* A **55** 1044–55
[30] Mukherjee T, Ghosh A S and Jain A 1991 Low-energy positron collisions with H_2 and N_2 molecules by using a parameter-free positron-correlation-polarization potential *Phys. Rev.* A **43** 2538–41
[31] Hake R D and Phelps A V 1967 Momentum-transfer and inelastic-collision cross sections for electrons in O_2, CO, and CO_2 *Phys. Rev.* **158** 70–84
[32] Nelson R D, Lide D R and Maryott A A (ed) 1967 *Selected Values of Electric Dipole Moments for Molecules in The Gas Phase* (Washington, DC: US National Bureau of Standards)
[33] Jain A 1990 A treatment of low-energy positron-co collisions using a new parameter-free positron correlation polarisation (pcop) potential *J. Phys. B: At. Mol. Phys.* **23** 863–84
[34] Ghosh A S and Mukherjee T 1996 Positron–molecule scattering at low and medium energies *Can. J. Phys.* **74** 420
[35] Tennyson J and Morgan L 1987 Rotational and polarization effects in low-energy positron-co collisions using the r-matrix method *J. Phys.* B **20** L641–646
[36] Bankovic A, Dujko S, White R D, Buckman S J and Petrovic Z Lj 2012 On approximations involved in the theory of positron transport in gases in electric and magnetic fields *Eur. Phys. J.* D **66** 174